

Oxide Characterization of Zr Alloys by Synchrotron Radiation Micro-Diffraction Method

150

synchrotron radiation micro-diffraction Zircaloy-4
 , Zircaloy-4
 가 ,
 25-40% /
 . FWHM Zircaloy-4 /

Abstract

Crystal structure, texture and stress distribution of oxide on the Zircaloy-4 have been investigated using synchrotron radiation micro-diffraction method. It was found that the oxide on the Zircaloy-4 consisted of monoclinic and tetragonal structures. The volume fraction of tetragonal phase was calculated to be 40% in oxide/metal interface and decreased to 25% in the region of surface. It was also found that the monoclinic phase was highly textured in oxide/metal interface. From the calculation of full width at half maximum for the monoclinic (200) peak, the internal stress in the oxide could be estimated. The internal stress was not significantly changed with oxide depth although it was measured to be higher somewhat in interface than in surface.

1.

Zr

Zr

. Zr

ZrO₂ , Zr (monoclinic structure) / 가 (ZrO₂)
 (tetragonal structure) 1000 , Zr¹⁾
 2)
 가 , 1)
 , 가 가 가
 가 가 가
 가 가
 Zr
 가
 synchrotron radiation
 Zr
 synchrotron radiation micro-diffraction / 가

2.

Zircaloy-4 (Zr-1.3wt.%Sn-0.2wt.%Fe-0.1wt.%Cr)
 25mm , 9.5mm Zircaloy-4
 , 5% HF, 45% HNO₃, 50% H₂O
 autoclave 360 water
 , 가 가
 가
 Synchrotron radiation micro-diffraction 가 1B2
 10 μm , 10X1 μm² ,
 12

keV 가 30mg/dm² 1.5μm 1.03A
 Fig. 1
 Fig. 1
 CCD

3.

Fig. 2 Zircaloy-4 CCD 가
 가
 Zr

$$\lambda = 2d \sin \theta \quad (1)$$

$$\theta = 0.5 \tan^{-1}(r/z) \quad (2)$$

Fig. 3 indexing (1) (2)

Zircaloy-4 (tetragonal structure) (monoclinic structure)

가 가

Fig. 4 Fig. 2 indexing Fig. 4

$$V_t = I_{t(101)} / (I_{m(-111)} + I_{t(101)} + I_{m(111)}) \quad (3)$$

Fig. 5 Fig. 5 25-40%

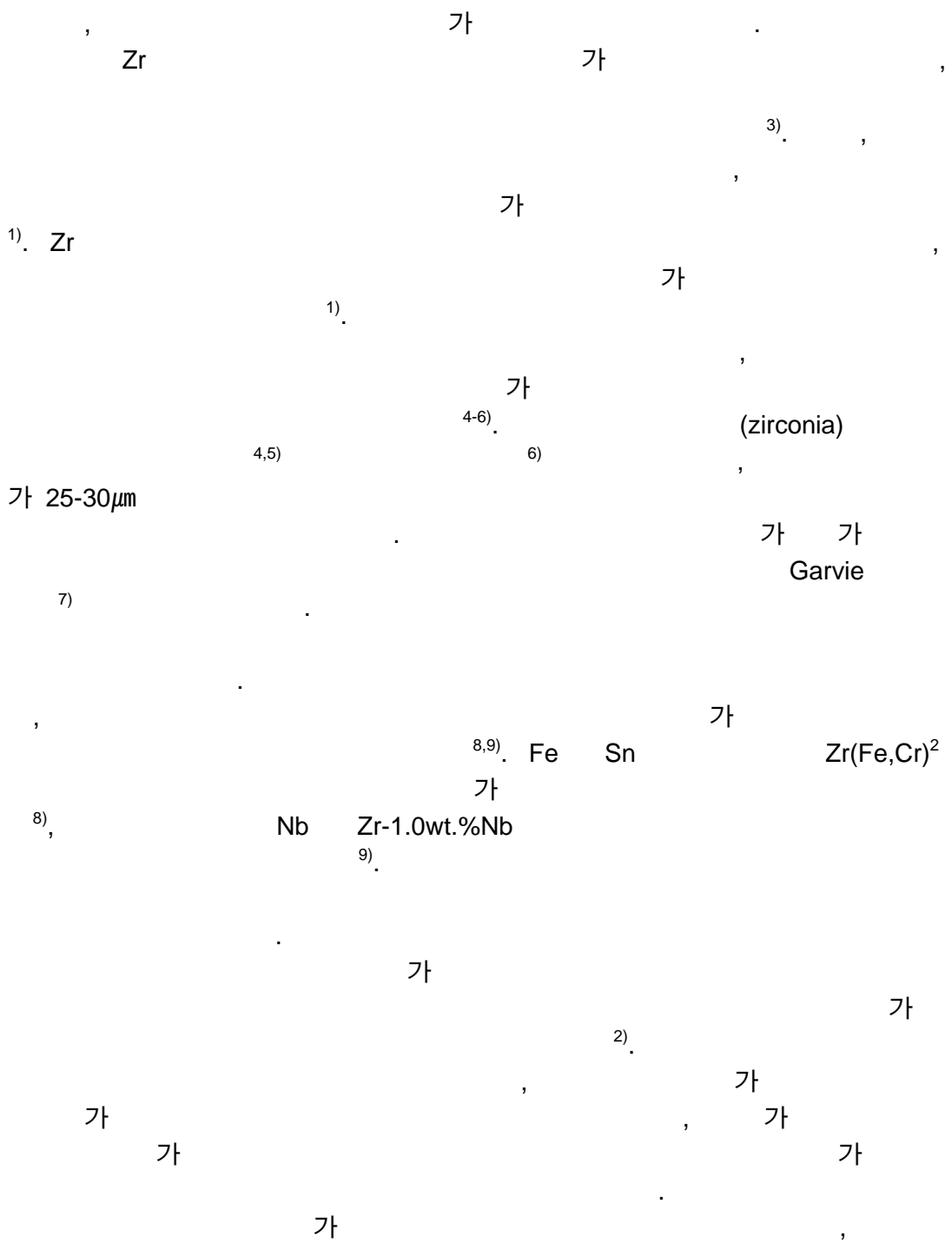


Fig. 6 monoclinic (200) full width at half maximum (FWHM)
 가 FWHM Fig. 6

synchrotron radiation micro-diffraction
가

Zr

4.

synchrotron radiation micro-diffraction

Zircaloy-4

Zircaloy-4

가

25-40%

/

/

FWHM

Zircaloy-4

- 1) J. Godlewski, Zirconium in the Nuclear Industry, ASTM STP 1245, 663 (1993).
- 2) J. Godlewski, J. P. Gros, M. Lambertin, J. F. Wadier and H. Weidinger, ASTM STP 1132, 416 (1991).
- 3) P. Barberis and A. Frichet, J. Nucl. Mater. 273, 182 (1999).
- 4) P. Barberis, J. Nucl. Mater. 226, 34 (1995).
- 5) E. Djurado, P. Bouvier and G. Lucazeau, J. Solid State Chem. 149, 399 (2000).
- 6) P. Bouvier and G. Lucazeau, J. Phys. Chem. Solids 61, 569 (2000).
- 7) R. C. Garvie, J. Phys. Chem. 69, 34 (1965).
- 8) P. Li, I. -W. Chen and J. E. Penner-Hahn, J. Am. Ceram. Soc. 77, 1281 (1994).
- 9) D. J. Kim, J. Am. Ceram. Soc. 73, 115 (1990).

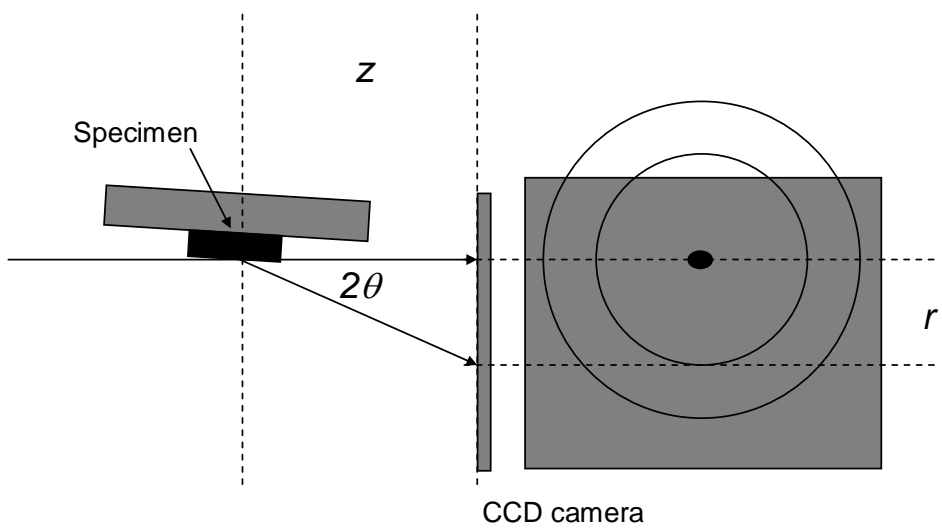


Fig. 1. Schematic diagram showing the geometry of data acquisition.

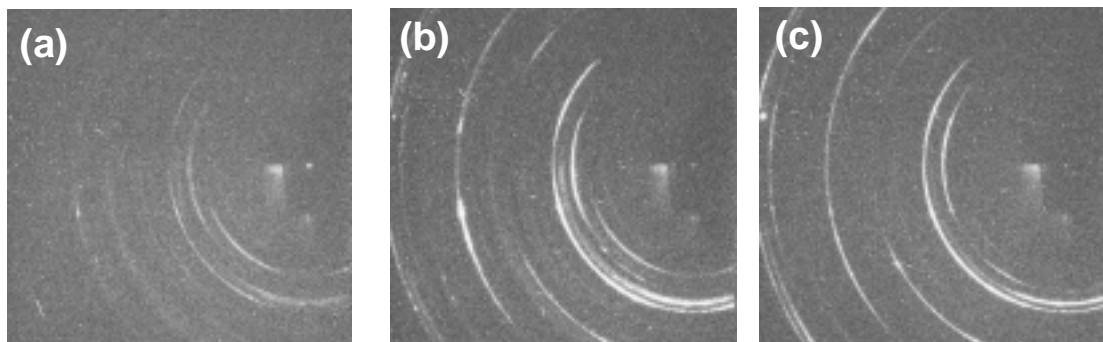


Fig. 2. Diffraction patterns from the region of (a) outer surface, (b) interior and (c) oxide/metal interface of oxide in the pre-transition regime.

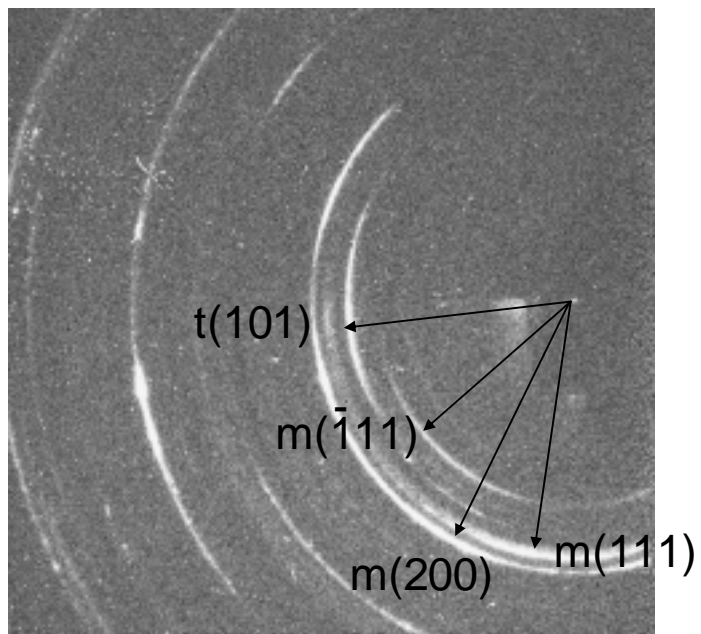


Fig. 3. Indexing of ring pattern. t and m represent tetragonal and monoclinic structures, respectively

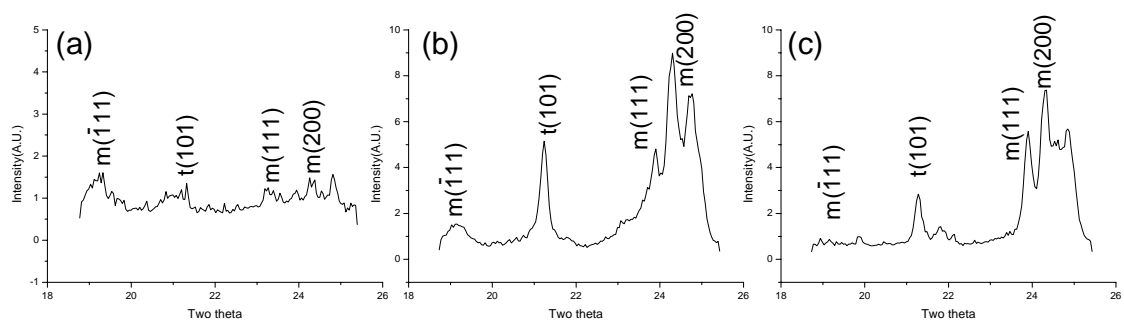


Fig. 4. Integrated intensity calculated from the diffraction pattern from region of (a) outer surface (b) interior and (c) interface on oxide in the prr-transition regime.

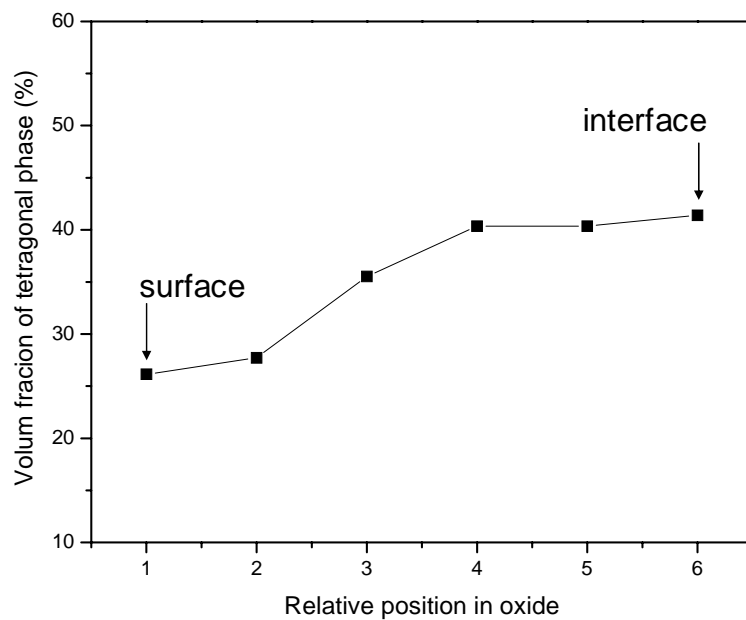


Fig. 5. Volume fraction of tetragonal phase calculated form integrated intensity.

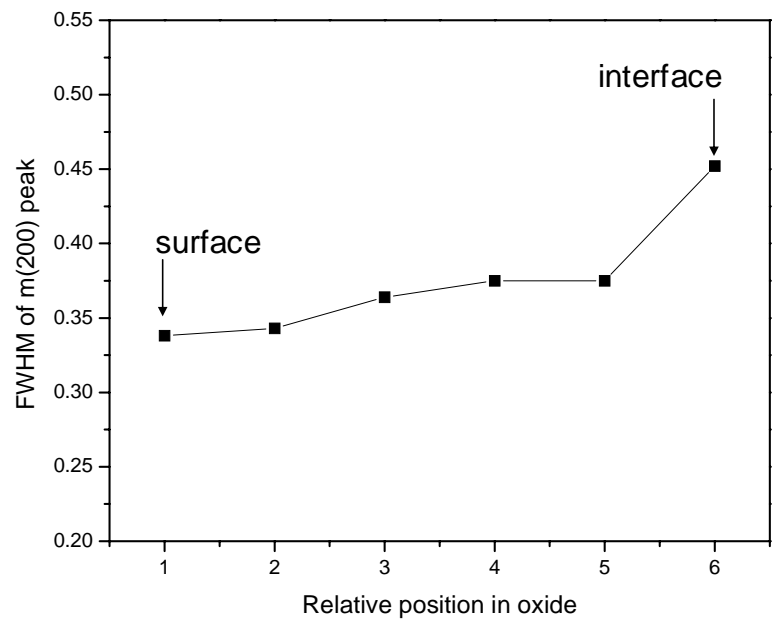


Fig. 6. Variation of full width at half maximum of monoclinic (200) peak with oxide position.